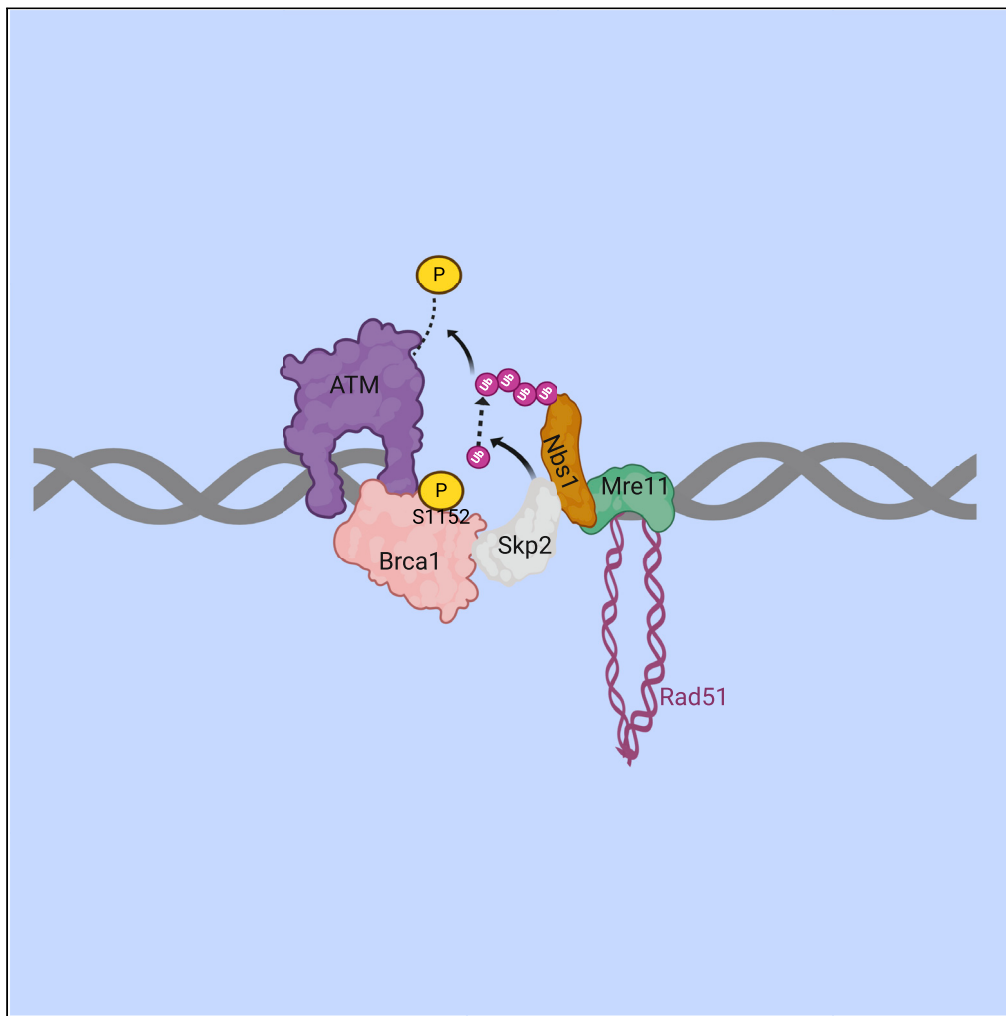Article

Phosphorylation of BRCA1 by ATM upon double-strand breaks impacts ATM function in end-resection: A potential feedback loop

Leilei Qi, Reka Chakravarthy, Monica M. Li, Chu-Xia Deng, Rong Li, Yanfen Hu

huy3@gwu.edu

Highlights

BRCA1-S1152A decreases mouse ATM phosphorylation and activity

BRCA1-Skp2-NBS1-ATM forms a feedback loop on ATM phosphorylation and activity

Mouse ATM-S1987 is not required for ATM phosphorylation and activity

Article

Phosphorylation of BRCA1 by ATM upon double-strand breaks impacts ATM function in end-resection: A potential feedback loop

Leilei Qi,[1,6] Reka Chakravarthy,[1,4,6] Monica M. Li,[1,5] Chu-Xia Deng,[3] Rong Li,[2] and Yanfen Hu[1,7,*]

SUMMARY

BRCA1 maintains genome stability by promoting homologous recombination (HR)-mediated DNA double-strand break (DSB) repair. Mutation of mouse BRCA1-S1152, corresponding to an ATM phosphorylation site in its human counterpart, resulted in increased genomic instability and tumor incidence. In this study, we report that BRCA1-S1152 is part of a feedback loop that sustains ATM activity. BRCA1-S1152A mutation impairs recruitment of the E3 ubiquitin ligase SKP2. This in turn attenuates NBS1-K63 ubiquitination by SKP2 at DSB, impairs sustained ATM activation, and ultimately leads to deficient end resection, the commitment step in the HR repair pathway. Auto-phosphorylation of human ATM at S1981 is known to be important for its kinase activation; we mutated the corresponding amino acid residue in mouse ATM (S1987A) to characterize potential roles of mouse ATM-S1987 in the BRCA1-SKP2-NBS1-ATM feedback loop. Unexpectedly, MEFs carrying the ATM-S1987A knockin mutation maintain damage-induced ATM kinase activation, suggesting a species-specific function of human ATM auto-phosphorylation.

INTRODUCTION

Germ-line mutations in *BRCA1* predispose women to breast and/or ovarian cancer (Abdulkarim et al., 2011). Since the identification of *BRCA1* gene in 1994, molecular studies have established that BRCA1 functions as a tumor suppressor, in large part, through its role in maintaining genome stability by promoting high fidelity, homologous recombination (HR)-mediated repair of DNA double-strand breaks (DSBs) (Zhang and Powell, 2005). Extensive characterizations reveal that BRCA1 forms multiple complexes with various DNA repair proteins at different stages of DNA damage response and repair (Huen et al., 2010). It is also well documented that upon DNA damage, BRCA1 protein is rapidly phosphorylated by multiple kinases involved in DNA repair and cell-cycle checkpoint controls such as ATM, CHK2, ATR etc. (Scully et al., 1997a) (Scully et al., 1997b) (Cortez et al., 1999) (Lee et al., 2000). Studies of human cell lines and genetically engineered mouse models showed that several of these phosphorylation sites are important for BRCA1 functions in DNA damage response (DDR). For example, we and others show that CHK2 phosphorylation of human BRCA1-S988 (or its corresponding mouse BRCA1-S971) is important for BRCA1's roles in maintenance of genome stability and promotion of HR-mediated DSB repair (Lee et al., 2000) (Kim et al., 2004) (Zhang et al., 2004) (Parameswaran et al., 2015). In particular, our published study shows that CHK2 phosphorylation of BRCA1-S971 coordinates end resection, the commitment step in HR pathway, to the S/G2 phases of the cell cycle through an elaborate "automation-like" mechanism (Parameswaran et al., 2015). However, compared with the extensive characterization of the dynamics of the DDR-induced BRCA1 protein complexes, the functionality of BRCA1 phosphorylation remains incompletely understood. In particular, it is unclear how multiple BRCA1 phosphorylation events by different kinases act in a functionally distinct and concerted manner to regulate its activity in HR-mediated DSB repair.

In response to DNA damage, BRCA1 is phosphorylated by the Ser/Thr protein kinase ATM at multiple serine residues, although the ATM phosphorylation sites mapped *in vivo* and *in vitro* are not completely identical (Cortez et al., 1999). ATM-dependent phosphorylation of human BRCA1-S1189 was initially identified *in vivo*, but its functional significance was not clear (Cortez et al., 1999). A follow-up study that mutated the corresponding residue in mouse BRCA1 (BRCA1-S1152A) showed that mice with the abrogated ATM phosphorylation site exhibited increased γ-irradiation (γIR)-induced tumorigenesis (Kim

[1]Department of Anatomy and Cell Biology, the George Washington University, School of Medicine and Health Sciences, Washington DC20037, USA

[2]Department of Biochemistry and Molecular Medicine, the George Washington University, School of Medicine and Health Sciences, Washington DC20037, USA

[3]Cancer Center, Faculty of Health Sciences, University of Macau, Macau, SAR China

[4]Present address: Department of Dermatology, Columbia University Irving Medical Center, New York, NY10032, USA

[5]Present address: Department of Medicine, School of Medicine, J. Willis Hurst Internal Medicine Residency Program, Emory University, Atlanta, Ga30322, USA

[6]These authors contributed equally

[7]Lead contact

*Correspondence: huy3@gwu.edu

https://doi.org/10.1016/j.isci.2022.104944

et al., 2009), suggesting that this evolutionarily conserved ATM phosphorylation site in BRCA1 is functionally important and likely plays roles in DDR and DSB repair. However, the molecular mechanism by which this particular ATM phosphorylation site supports BRCA1 function was not understood. Specifically, it is not known whether this phosphorylation event influences BRCA1 activity through a different mechanism from the aforementioned CHK2-mediated phosphorylation event (Parameswaran et al., 2015).

To elucidate the functional impact of ATM phosphorylation of BRCA1-S1152 on HR-mediated DNA DSB repair, we used mouse embryonic fibroblasts (MEFs) derived from BRCA1-S1152A KI mutant embryos in a comparative study with those carrying the S971A mutation. We found that similar to what has been observed in *Brca1^{S971A/S971A}* MEFs, abrogation of BRCA1-S1152 phosphorylation impaired end resection without affecting the assembly of end resection complex MRE11, RAD50, and CtIP at DSBs. However, unlike *Brca1^{S971A/S971A}* MEFs, *Brca1^{S1152A/S1152A}* cells were defective in sustaining the ATM kinase activity, suggesting a potential positive feedback loop. In addition, our study also shed light on a species-specific function of ATM auto-phosphorylation. Thus, our results provide compelling evidence for distinct and nuanced roles of different BRCA1 phosphorylation events in orchestrating end resection in HR-mediated DSB repair.

RESULTS

Abrogation of ATM phosphorylation on mouse BRCA1-Ser1152 impairs end resection

To determine whether phosphorylation of mouse BRCA1-S1152 impacts end resection in HR-mediated DSB repair, two pairs of MEFs (*Brca1^{WT}* and *Brca1^{S1152A/S1152A}*) from independent breeding were immortalized. Upon confirming that the BRCA1 expression levels and cell cycle distributions were compatible between WT and mutant MEFs (data not shown and Figure S1), we examined the impact of BRCA1-S1152A mutation on end resection and assembly of protein complexes involved in end resection. First, we used BrdU-dependent laser microirradiation, followed by indirect immunofluorescence (IF) staining of RAD51 (Parameswaran et al., 2015). RAD51 is one of the key players in the HR-mediated DSB repair pathway. RAD51 is recruited to DSBs to "coating" single-stranded DNA (ssDNA) generated from end resection, a commitment step that serves as an initiation of the HR pathway. Therefore, RAD51 recruitment to laser-induced DSBs signifies successful end resection. As demonstrated by our published work (Parameswaran et al., 2015), the experimental condition used in this assay limits laser-induced DSBs to cells at the S/G2 phases of the cell cycle, when HR-mediated DSB repair normally occurs (also see "STAR Methods" for details).

Both *Brca1^{WT}* and *Brca1^{S1152A/S1152A}* MEF cells were subject to BrdU-dependent laser microirradiation. Presence of RAD51 at DSBs at 10, 30, and 60 min after microirradiation was visualized by indirect immunofluorescence (Figure 1A top panel). γH2AX (green stripes) serves as a readout for microirradiation-generated DSBs, whereas RAD51 (red stripes) indicates execution of end resection at DSBs. The percentage of RAD51+/γH2AX+ cells reflects the overall efficiency of end resection after microirradiation (Figure 1A graph at the bottom). End resection efficiency was significantly lower in *Brca1^{S1152A/S1152A}* MEFs versus *Brca1^{WT}* MEFs at the two early time points (10 and 30 min), suggesting a delay or lower efficiency in DSB repair.

Besides RAD51 recruitment to DSBs, detection of BrdU-labeled ssDNA can also serve as a readout of successful end resection (Parameswaran et al., 2015). Under this particular assay condition (see STAR Methods), BrdU serves a different purpose. Laser microirradiation was conducted in a BrdU-independent manner to ensure that BrdU positivity reflects only efficiency of end resection, not that of DSB generation. Importantly, BrdU incorporated into DNA is detectable with BrdU antibodies only when DNA is in single-stranded form. As a result, BrdU immunostaining could detect ssDNA generated by end resection, but not their double-stranded counterpart (Figure 1B). Consistent with the findings from the RAD51-based assay (Figure 1A), the percentage of BrdU+/γH2AX+ was also lower in mutant MEFs than their WT counterpart (Figure 1B graph at bottom panel). Because *Brca1^{WT}* and *Brca1^{S1152A/S1152A}* MEFs have very similar cell-cycle distribution (Figure S1), the difference in BrdU stripes reflects intrinsic difference in end resection efficiency upon microirradiation, rather than difference in percentage of S/G2 cells. Taken together, these results clearly support the notion that BRCA1-S1152 phosphorylation is required for efficient end resection.

To further corroborate impaired end resection in *Brca1^{S1152A/S1152A}* MEF cells, we assessed IR-induced phosphorylation of CHK1-S345 and RPA2-S4/8, which occurs downstream of end resection in the HR pathway. The levels of CHK1-S345 and RPA2-S4/8 phosphorylation correlate with end resection as well.
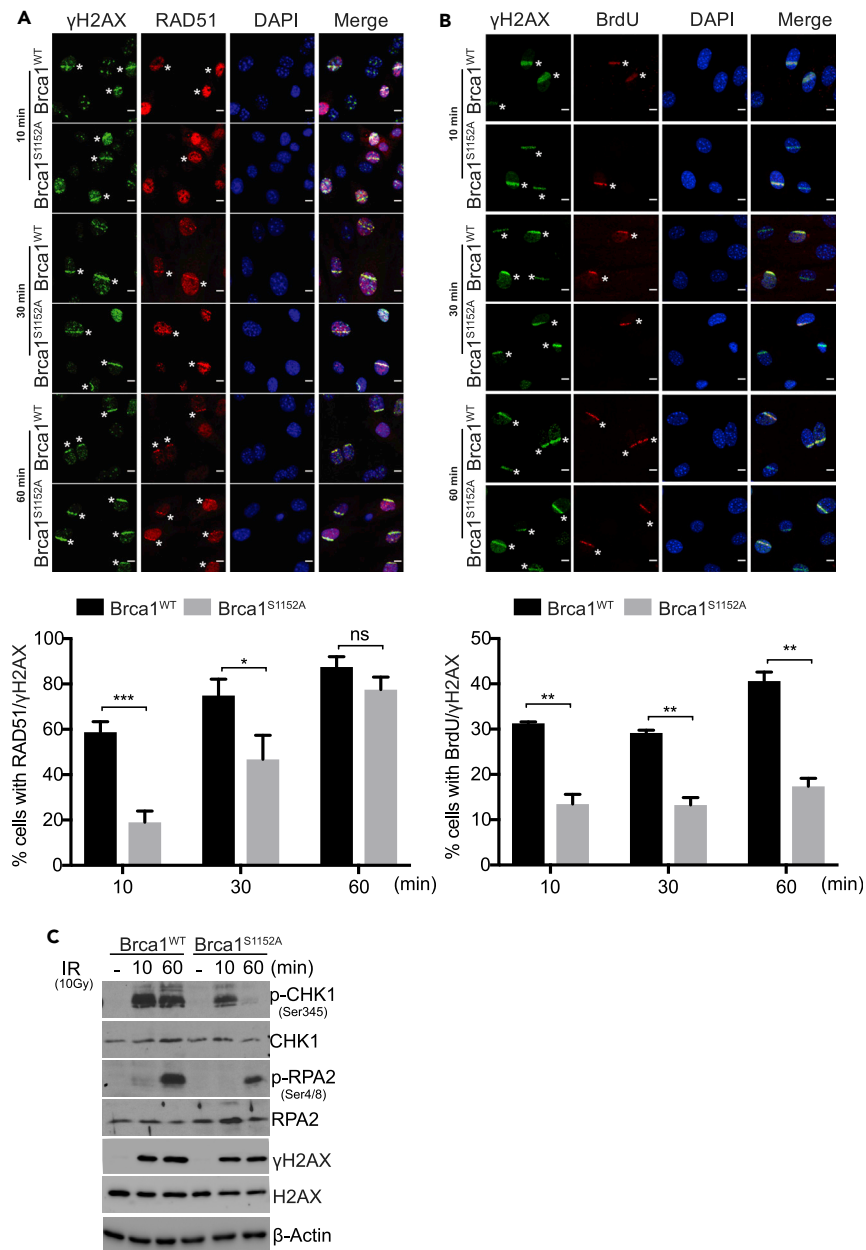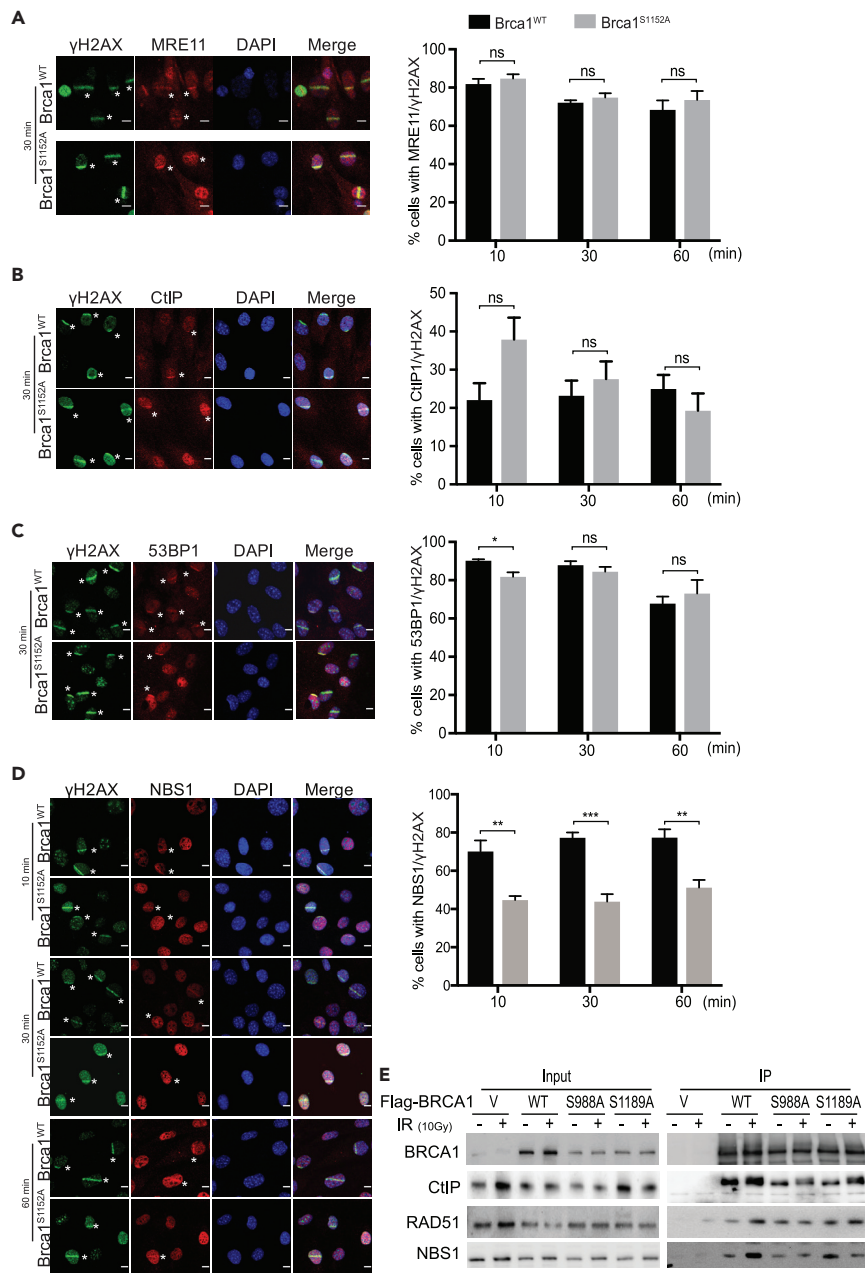
Figure 1. Abrogation of ATM phosphorylation on BRCA1-S1152 impairs end resection

(A) RAD51 recruitment upon microirradiation. RAD51 laser stripes (red) and γH2AX (green) from S/G2 cells at 10, 30, and 60 min after microirradiation. Scale bar, 10 μm. Bar graph shows quantification of laser stripes. Average from 6 independent experiments. 10 min (n = 248 for $Brca1^{WT}$ and n = 165 for $Brca1^{S1152A/S1152A}$, p = 7.58164 × 10^{-5}); 30 min (n = 201 for $Brca1^{WT}$ and n = 140 for $Brca1^{S1152A/S1152A}$, p = 0.026263168); 60 min (n = 290 for $Brca1^{WT}$ and n = 292 for $Brca1^{S1152A/S1152A}$, p = 0.09250862).

(B) Detection of ssDNA upon microirradiation. BrdU (ssDNA) stripes (red) and γH2AX (green) from total cell population at 10, 30, and 60 min time points after microirradiation. Scale bar, 10 μm. Bar graph shows quantification of laser stripes. Average from 3 independent experiments. 10 min (n = 594 for $Brca1^{WT}$ and n = 803 for $Brca1^{S1152A/S1152A}$, p = 0.003895929); 30 min (n = 529 for $Brca1^{WT}$ and n = 809 for $Brca1^{S1152A/S1152A}$, p = 0.002853738); 60 min (n = 653 for $Brca1^{WT}$ and n = 912 for $Brca1^{S1152A/S1152A}$, p = 0.003046438).

(C) Phosphorylation of CHK1and RPA32, but not of H2AX, is impaired in $Brca1^{S1152A/S1152A}$ MEFs 10 and 60 min after IR (10 Gy).

Figure 2. Abrogation of ATM phosphorylation on BRCA1-S1152 affects assembly of NBS1 but not on the recruitment of MRE11/CtIP/53BP1 upon DNA damage

Recruitment of MRE11 (A), CtIP (B), 53BP1 (C), and NBS1 (D) after microirradiation in BRCA1 WT and S1152A MEF cells. Laser stripes of indicated proteins (red) and γH2AX (green) from S/G2 cells at 10, 30, and 60 min time points. Scale bar, 10 μm. Bar graph shows quantification of laser strips. Average from 3 to 4 independent experiments. For MRE11: 10 min (n = 452 for $Brca1^{WT}$ and n = 437 for $Brca1^{S1152A/S1152A}$, p = 0.1176); 30 min (n = 405 for $Brca1^{WT}$ and n = 433 for $Brca1^{S1152A/S1152A}$, p = 0.0695); 60 min (n = 511 for $Brca1^{WT}$ and n = 676 for $Brca1^{S1152A/S1152A}$, p = 0.1299). These data are from 3 independent experiments. For 53BP1: 10 min (n = 534 for $Brca1^{WT}$ and n = 687 for $Brca1^{S1152A/S1152A}$, p = 0.007104); 30 min (n = 436 for $Brca1^{WT}$ and n = 407 for $Brca1^{S1152A/S1152A}$, p = 0.170465); 60 min (n = 543 for $Brca1^{WT}$ and n = 386 for $Brca1^{S1152A/S1152A}$, p = 0.267004). The data are from 4 independent experiments. For CtIP: 10 min (n = 147 for $Brca1^{WT}$ and n = 170 for $Brca1^{S1152A/S1152A}$, p = 0.024461); 30 min (n = 115 for $Brca1^{WT}$ and n = 215 for $Brca1^{S1152A/S1152A}$, p = 0.251565); 60 min (n = 103 for $Brca1^{WT}$ and n = 214 for $Brca1^{S1152A/S1152A}$, p = 0.178625). The data are from 4 independent experiments. For NBS1, 10 min (n = 125 for $Brca1^{WT}$ and n = 102 for $Brca1^{S1152A/S1152A}$, p = 0.002956746); 30 min (n = 203

Figure 2. *Continued*

for $Brca1^{WT}$ and n = 174 for $Brca1^{S1152A/S1152A}$, p = 0.000222756); 60 min (n = 159 for $Brca1^{WT}$ and n = 165 for $Brca1^{S1152A/S1152A}$, p = 0.002122252).

(E) Interaction of BRCA1 with RAD51 and CtIP is comparable among Flag-tagged human BRCA1 (WT, S1189A, and S988A) as shown in coimmunoprecipitation assay in HEK293 cells. However, interaction between NBS1 and Flag-BRCA1-S1189A is reduced after IR.

Consistent with the findings from the laser microirradiation experiments, phosphorylation of CHK1-S345 and RPA2-S4/8 10 and 60 min after γ-irradiation was significantly weaker in mutant MEF cells than their WT control (Figure 1C).

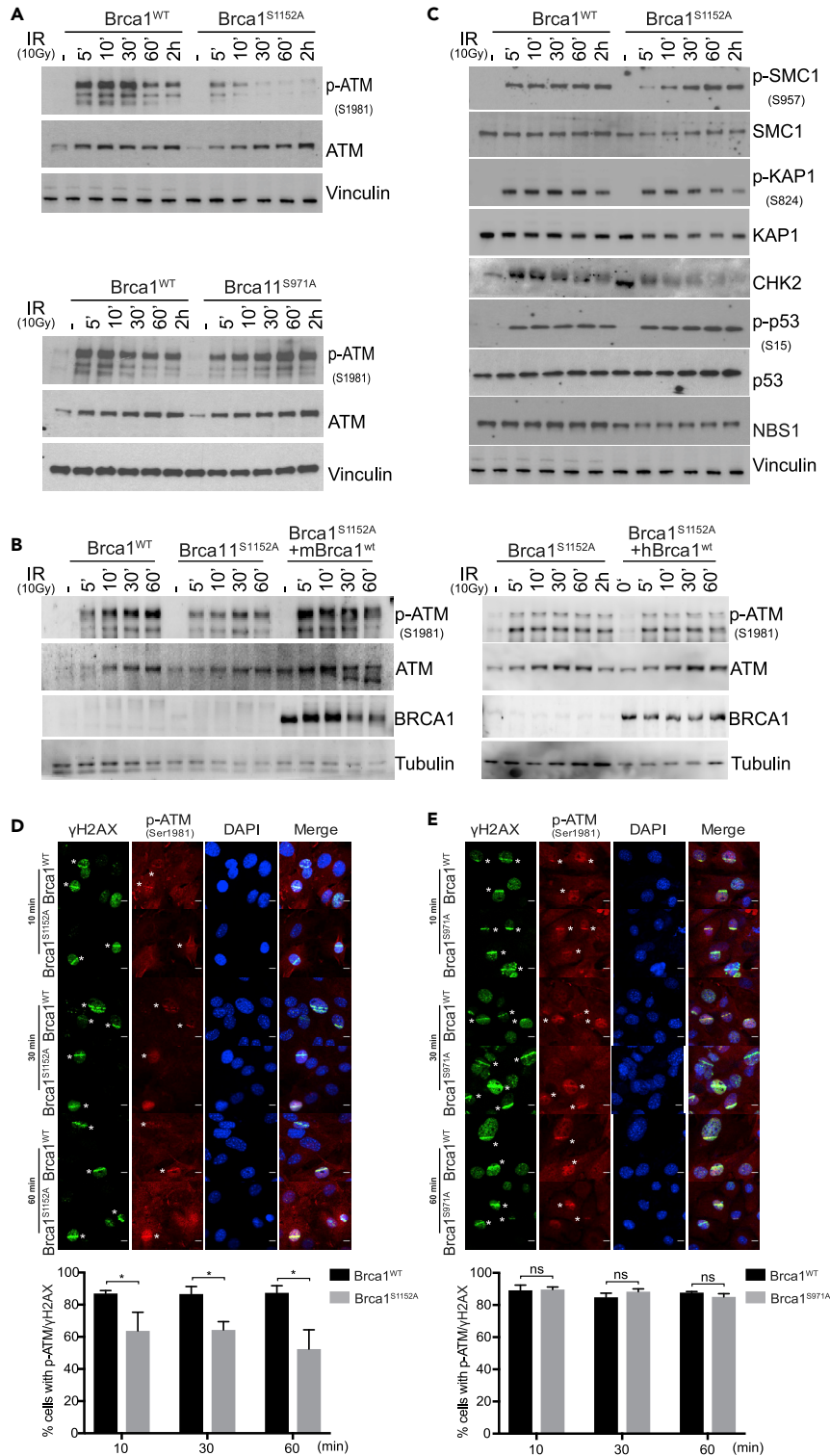## Abrogation of phosphorylation on mouse BRCA1-S1152 has differential impact on assembly of MRN, CtIP, and 53BP1

To elucidate the mechanism underlying impaired end resection in $Brca1^{S1152A/S1152A}$ MEF cells, we examined assembly of MRE11, NBS1, CtIP, and 53BP1 at DSBs, as these proteins have been shown to play important roles in end resection and regulate choice of repair pathways between HR and non-homologous end-joining (NHEJ). Microirradiation followed by indirect immunofluorescence showed that recruitment of MRE11, CtIP, and 53BP1 at DSBs was statistically indistinguishable between $Brca1^{WT}$ and $Brca1^{S1152A/S1152A}$ cells at all time points after microirradiation (Figures 2A–2C). In contrast, recruitment of NBS1 at DSBs was consistently slower in $Brca1^{S1152A/S1152A}$ cells than their WT control at all three time points (Figure 2D). This is different from abrogation of CHK2 phosphorylation of mouse BRCA1-S971, which does not affect assembly of MRE11-RAD50-NBS1, CtIP, or 53BP1 (Parameswaran et al., 2015). Our previous work showed physical association between BRCA1 and NBS1 (Parameswaran et al., 2015). We therefore used coimmunoprecipitation to compare the affinity of human WT and mutant BRCA1 (S1189A and S988A corresponding to mouse S1152A and S971A, respectively) for NBS1, before and after γ-irradiation. Flag-tagged human BRCA1 was transiently expressed in HEK293T cells and immunoprecipitated with an anti-Flag antibody. Although WT and BRCA1-S988A retained the binding affinity for NBS1 in irradiated cells, much less NBS1 was coimmunoprecipitated with BRCA1-S1189A after γ-irradiation versus prior (Figure 2E). Collectively, these data suggest a distinct role of ATM phosphorylation of BRCA1 in NBS1 recruitment during end resection.

Abrogation of phosphorylation on mouse BRCA1-S1152 impairs ATM phosphorylation

We examined impact of abrogation of mouse BRCA1-S1152 phosphorylation on ATM phosphorylation and activation, a molecular event upstream of end resection in HR-mediated DSB repair. Phosphorylation of human ATM-S1981, which corresponds to mouse ATM-S1987, has been well established as a marker for human ATM kinase activation (Bakkenist and Kastan, 2003) (Shiloh and Ziv, 2013) (Blackford and Jackson, 2017) (Lee and Paull, 2021). One human anti-ATM-pS1981 antibody is commonly used to detect mouse ATM activation (Pellegrini et al., 2006) (Stracker et al., 2007) (Tian and Mao, 2009) (Wu et al., 2012) (Lim et al., 2013), whereas another published antibody raised against mouse ATM-pS1987 is no longer available (Manuela Pellegrini and Andre Nussenzweig, personal communication) (Pellegrini et al., 2006). We therefore used the human anti-ATM-pS1981 antibody in a time course study of ATM phosphorylation/activation following γ-irradiation of BRCA1 WT and mutant MEFs ($Brca1^{WT}$, $Brca1^{S1152A/S1152A}$, and $Brca1^{S971A/S971A}$). Consistent with our previously published work (Parameswaran et al., 2015), abrogation of CHK2 phosphorylation on BRCA1-S971 did not affect IR-induced ATM phosphorylation (Figure 3A bottom panel). In contrast, ATM phosphorylation upon γ-irradiation was significantly impaired in $Brca1^{S1152A/S1152A}$ cells (Figure 3A top panel). To ascertain that the impaired ATM phosphorylation in $Brca1^{S1152A/S1152A}$ MEFs was indeed due to the loss of BRCA1 function, mouse WT BRCA1 was overexpressed in $Brca1^{S1152A/S1152A}$ MEF cells. Expression of exogenous mouse WT BRCA1 restored IR-induced ATM phosphorylation to the levels comparable to that in parental WT MEFs (Figure 3B left panel), corroborating a direct causal relationship between mouse BRCA1-S1152A and ATM phosphorylation. Intriguingly, overexpression of human WT BRCA1 did not restore ATM phosphorylation in $Brca1^{S1152A/S1152A}$ MEFs (Figure 3B right panel), suggesting human and mouse BRCA1 proteins are not interchangeable in this functional readout.

Next, we investigated whether impaired ATM phosphorylation in $Brca1^{S1152A/S1152A}$ cells affects ATM kinase activity. To this end, we assessed phosphorylation of several known ATM substrates upon γ-irradiation, including SMC1, p53, KAP1, and CHK2. Phosphorylation of SMC1 and tumor suppressor p53 was not affected and that of KAP1 was only mildly decreased in $Brca1^{S1152A/S1152A}$ MEFs (Figure 3C). In contrast,

Figure 3. Abrogation of ATM phosphorylation on BRCA1-S1152 affects the kinetics of ATM activation in response to DNA damage

(A) The kinetics of ATM phosphorylation/activation is affected in $Brca1^{S1152A/S1152A}$ MEF cells, but not in $Brca1^{S971A/S971A}$ MEF cells, compared with $Brca1^{WT}$ cells. Overexpression of mouse WT BRCA1 (B top), but not human WT BRCA1 (B

Figure 3. *Continued*

bottom), in *Brca1^S1152A/S1152A* MEF cells restores ATM activation. The ATM doublet on the blot appears only when samples are loaded near the edge of a gel. This position effect is not fully understood.

(C) Phosphorylation of ATM substrates in *Brca1^WT* and *Brca1^S1152A/S1152A* MEF cells. CHK2 phosphorylation can be detected using CHK2 antibody as phosphorylation caused upshift of CHK2 position.

(D) Recruitment of phospho-ATM is partially impaired in *Brca1^S1152A/S1152A* MEF but not in *Brca1^S971A/S971A* MEF. (E) Phospho-ATM laser stripes (red) and γH2AX (green) from S/G2 cells. Scale bar, 10 μm. For S1152A pair: 10 min (n = 124 for *Brca1^WT* and n = 138 for *Brca1^S1152A/S1152A*, p = 0.03552); 30 min (n = 125 for *Brca1^WT* and n = 127 for *Brca1^S1152A/S1152A*, p = 0.01515); 60 min (n = 101 for *Brca1^WT* and n = 100 for *Brca1^S1152A/S1152A*, p = 0.01803). Bar graph is average of 4 independent experiments. For S971A pair: 10 min (n = 260 for *Brca1^WT* and n = 188 for *Brca1^S971A/S971A*, p = 0.451564); 30 min (n = 308 for *Brca1^WT* and n = 302 for *Brca1^S971A/S971A*, p = 0.192651); 60 min (n = 290 for *Brca1^WT* and n = 107 for *Brca1^S971A/S971A*, p = 0.17004). Bar graph is average of 2 independent experiments.

phosphorylation of CHK2 was substantially reduced in mutant MEFs at all time points examined (shifted bands in Figure 3C). These results suggest that the impact of ATM phosphorylation on its kinase activity is substrate dependent in MEFs.

Lastly, we examined how impaired ATM phosphorylation affects its own recruitment to DSBs. BRCA1 WT and mutant MEFs were subject to laser microirradiation followed by indirect immunofluorescence using the anti-human ATM-pS1981 antibody (Figure 3D). Laser microirradiation was conducted in a BrdU-dependent manner to capture initial DDR steps in S/G2 cells. Our results showed that the presence of phosphorylated ATM at DSBs was reduced in *Brca1^S1152A/S1152A* versus *Brca1^WT* MEFs at all three time points (Figure 3D, 10, 30, and 60 min). In contrast, *Brca1^S971A/S971A* MEFs and their WT counterparts exhibited no difference in recruitment of phosphorylated ATM at DSBs (Figure 3E), indicating that BRCA1-S1152 phosphorylation is uniquely important for recruitment of phosphorylated ATM to DSBs.

"SKP2-NBS1 ubiquitination-ATM activation" circuit is impaired in *Brca1^S1152/S1152A* MEF cells

It was previously reported that the E3 ubiquitin ligase SKP2 integrates ATM activation in HR-mediated DNA repair through its K63-linked ubiquitination of NBS1 (Wu et al., 2012). The connection between ATM and MRN complex is thought to be a central functional link during ATM activation (Shiloh and Ziv, 2013). Unlike K48-linked ubiquitination, K63-linked ubiquitination does not mediate protein degradation. Rather, it is involved in protein-protein interaction (Wu et al., 2012). Reduced NBS1-K63 ubiquitination leads to weakened interaction between ATM and NBS1, which in turn results in deficient ATM activation (Wu et al., 2012). Our own published results also established that SKP2 interacts with BRCA1 in cell extract and at DSBs (Lu et al., 2012) (Parameswaran et al., 2015). We therefore speculated that BRCA1-S1152A might weaken interaction between BRCA1 and SKP2, which could account for reduced recruitment of NBS1 (Figures 2D and 2E) and activation of ATM (Figure 3). Due to lack of quality SKP2 antibody that recognizes mouse SKP2 in IP-Western assay (data not shown), we examined interaction between human Flag-BRCA1 and endogenous SKP2 in HEK293T cells. Flag-BRCA1 (WT, S988A, S1189A) was immunoprecipitated with an anti-Flag antibody, and the level of associated endogenous SKP2 was compared. Our results showed that interaction between BRCA1-S1189A (corresponding to mouse BRCA1-S1152A) and SKP2 was significantly reduced following γ-IR, whereas that of WT and BRCA1-S988A was either not affected or even slightly increased (Figure 4A). In addition, we found by laser microirradiation/IF that recruitment of SKP2 to DSBs was much slower in *Brca1^S1152A/S1152A* MEFs than their WT counterparts (Figure 4B). Together these data support the notion that BRCA1-S1152 is important for BRCA1-dependent SKP2 recruitment to DSB repair events.

Next, we determined whether SKP2-mediated NBS1-K63 ubiquitination is affected in *Brca1^S1152A/S1152A* MEFs. Endogenous NBS1 was immunoprecipitated, and its K63-linked ubiquitination was detected using an antibody against K63-ubiquitination. Consistent with the published findings, NBS1-K63 ubiquitination in *Brca1^WT* cells was significantly increased upon γ-IR (compare lane 1 and 2 in Figure 4C). In contrast, the level of NBS1-K63 ubiquitination in *Brca1^S1152A/S1152A* cells was noticeably lower than that in the WT control (compare lane 2 and 4 in Figure 4C). As a comparison, there was no decrease in NBS1-K63 ubiquitination in *Brca1^S971A/S971A* cells in response to γ-IR (lanes 5–8 in Figure 4C). Thus, BRCA1-S1152 plays a unique role in facilitating NBS1-K63 ubiquitination.

Lastly, we examined the impact of BRCA1-S1152A on the interaction between NBS1 and phospho-ATM. As expected, co-IP showed that in *Brca1^WT* MEFs, γ-IR resulted in more ATM phosphorylation and
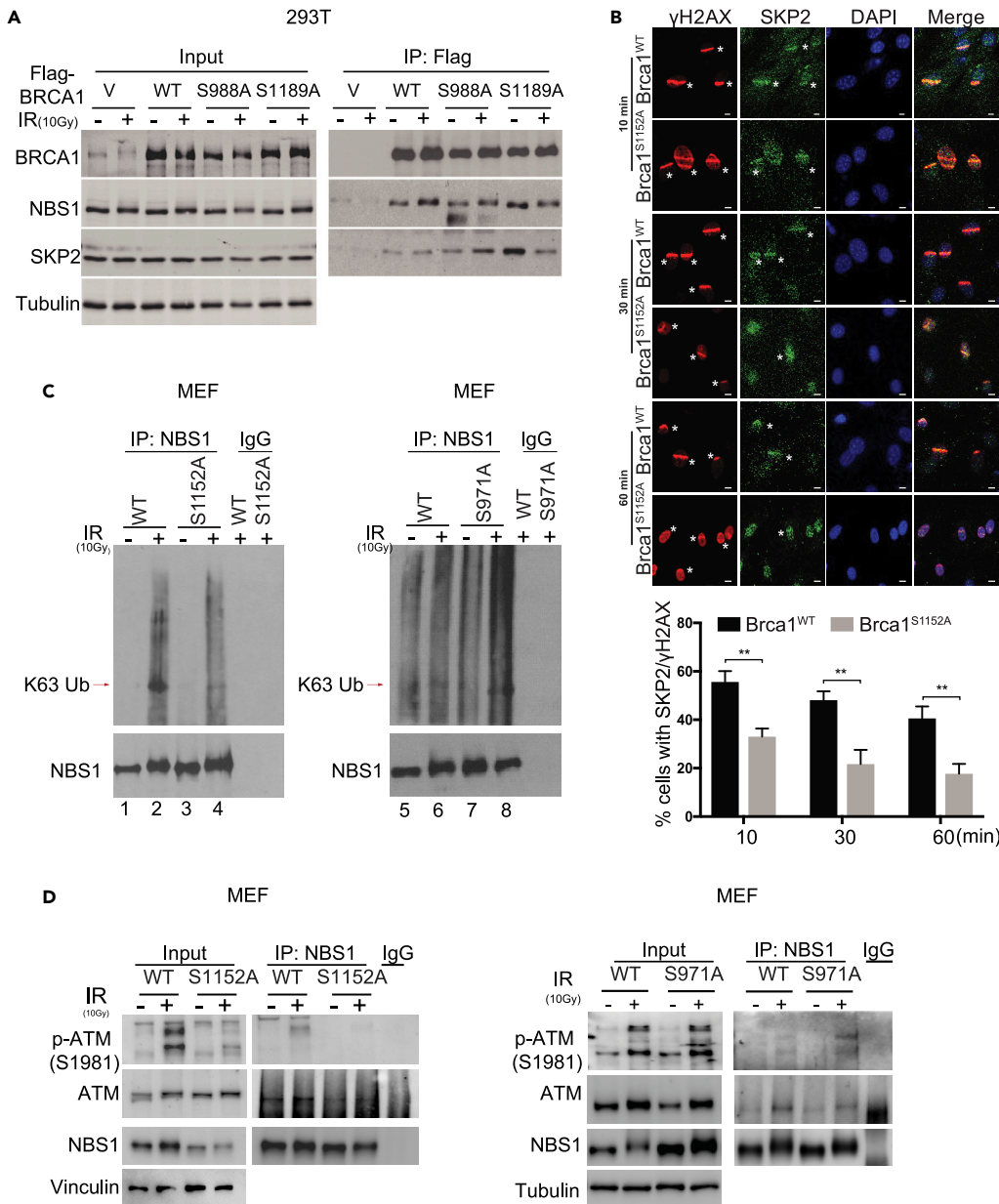
Figure 4. Abrogation of ATM phosphorylation on BRCA1-S1152 reduces SKP2 recruitment and ATM-NBS1 interaction upon DNA damage

(A) Coimmunoprecipitation shows reduced interaction between BRCA1-S1198A and SKP2 in HEK293 cells.

(B) Recruitment of SKP2 upon microirradiation. SKP2 laser stripes (green) and γH2AX (red) at 10, 30, and 60 min time points are shown. Scale bar, 10 μm. Bar graph below is quantification of three independent experiments. For 10 min (n = 326 for $Brca1^{WT}$ and n = 351 for $Brca1^{S1152A/S1152A}$, p = 0.007656); 30 min (n = 336 for $Brca1^{WT}$ and n = 427 for $Brca1^{S1152A/S1152A}$, p = 0.009519); 60 min (n = 336 for $Brca1^{WT}$ and n = 380 for $Brca1^{S1152A/S1152A}$, p = 0.009258).

(C) Immunoprecipitation of endogenous NBS1 shows reduced K63-linked ubiquitination of NBS1 in $Brca1^{S1152A/S1152A}$ MEF cells, but not in $Brca1^{S971A/S971A}$ MEF cells, in response to DNA damage.

(D) Coimmunoprecipitation shows reduced interaction between NBS1 and ATM upon DNA damage in $Brca1^{S1152A/S1152A}$ MEF cells but not in $Brca1^{S971A/S971A}$ MEF cells.

NBS1-associated phospho-ATM (Figure 4D). However, much less NBS1-associated phospho-ATM was detected in $Brca1^{S1152A/S1152A}$ cells compared with their WT counterparts (Figure 4D; left panel). Of note, $Brca1^{S971A/S971A}$ MEFs did not display a similar decrease in NBS1-associated phospho-ATM (Figure 4D;
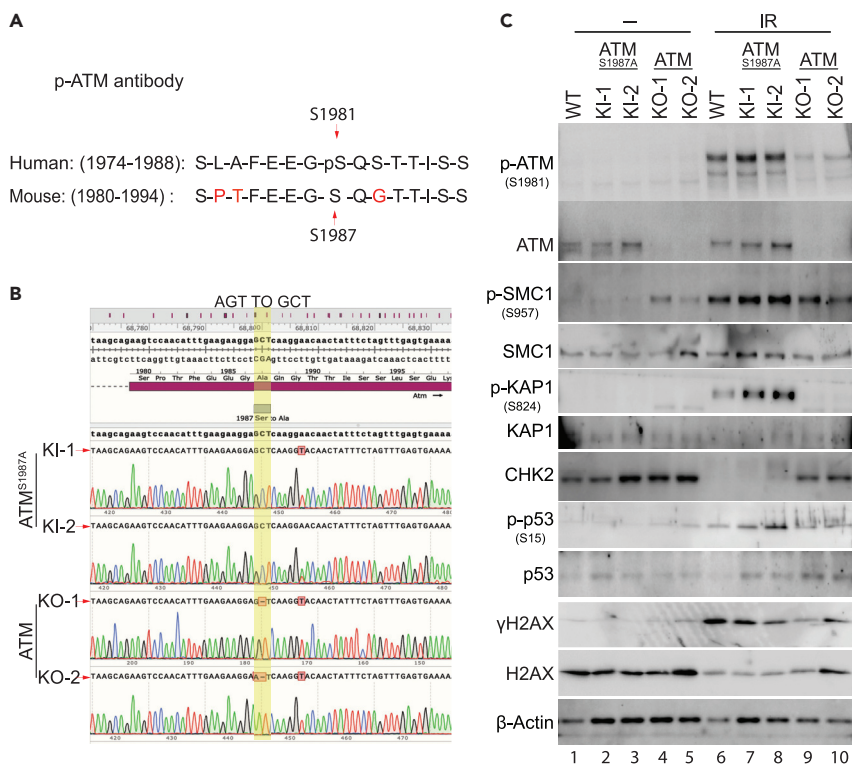
Figure 5. Mouse ATM Ser1987 is not required for ATM kinase activity

(A) Predicted human and mouse ATM recognizing sites for phospho-ATM antibody.

(B) DNA sequence of CRISPR/Cas9-mediated ATM-S1987A knockin (KI) and ATM knockout (KO) clones derived from wild-type MEF.

(C) Activation of ATM kinase activity 45 min after IR in ATM WT, KI, and KO MEF cells. Note that CHK2 phosphorylation caused upshift of CHK2 from a discrete band to cluster of bands.

right panel), supporting a unique role of BRCA1-S1152 in influencing the link between ATM and the MRN complex. Taken together, our data suggest that BRCA1-S1152 facilitates positive feedback in a previously established functional circuit that involves SKP2-NBS1 ubiquitination-ATM activation (Wu et al., 2012).

Abrogation of mouse ATM-S1987 phosphorylation does not impact ATM kinase activity

It has been well documented that phosphorylation of human ATM-S1981, which corresponds to mouse ATM-S1987, is both a marker and prerequisite for its kinase activation (Bakkenist and Kastan, 2003) (Lee and Paull, 2021). Of note, the amino acid sequences flanking mouse ATM-S1987 and human ATM-S1981 are not identical (Figure 5A). Furthermore, the role of mouse ATM-S1987 phosphorylation in HR-mediated repair remains controversial (Pellegrini et al., 2006) (Lee and Paull, 2021). The same phospho-Ser antibody raised against human ATM-pS1981 has been commonly used as a marker for mouse ATM activation (Pellegrini et al., 2006) (Stracker et al., 2007) (Tian and Mao, 2009) (Wu et al., 2012) (Lim et al., 2013). To determine whether γIR-induced ATM phosphorylation as detected by the anti-human phospho-ATM antibody was indeed due to ATM-S1987 phosphorylation, we generated ATM-S1987A knockin (KI) mutation in $Brca1^{WT}$ MEFs using CRISPR/Cas9 genome editing method (Figure 5B). In the process of generating $Atm^{S1987A/S1987A}$ KI MEFs, we also obtained ATM knockout (KO) clones, due to indels in the sgRNA-targeted DNA region.

Two independent KI and KO clones (designated as ATM KI-1, KI-2, KO-1, KO-2, in Figure 5B) and their WT counterpart were compared for ATM phosphorylation and kinase activity (Figure 5C). To our surprise, ATM phosphorylation in response to γ-IR, as detected by the anti-human-ATM-pS1981 antibody, was not affected at all in $Atm^{S1987A/S1987A}$ KI MEFs compared with parental WT cells (compare lanes 7 and 8 with 6 in top panel of Figure 5C). In ATM KO MEFs, the total ATM band was absent as expected (lanes 9 and 10 of top second panel in Figure 5C). The γIR-induced phospho-ATM band was significantly reduced,

although a faint band at the phospho-ATM position could still be detected by the anti-human ATM-pS1981 antibody, suggesting a low level of antibody cross-reactivity (Figure 5C top panel, lanes 9 and 10). These data strongly suggest that, contrary to prevalent assumption, the anti-human-ATM-pS1981 antibody most likely detects mouse ATM phosphorylation independent of S1987. In addition, γIR-induced phosphorylation of ATM kinase substrates, including SMC1, KAP1, CHK2, p53, and H2AX, was as effective in $Atm^{S1987A/S1987A}$ KI MEFs as in WT MEFs (Figure 5C lanes 6–8), thus supporting the notion that S1987 is not required for ATM kinase activation. In ATM KO MEFs, γIR-induced phosphorylation of KAP1 and CHK2 was barely detectable, whereas that of SMC1 and p53 was reduced as compared with WT MEFs (compare lanes 9 and 10 with 6 in Figure 5C). The presence of low level of SMC1 and p53 phosphorylation in the absence of ATM suggests there might be ATM-independent alternative pathways in MEFs to phosphorylate SMC1 and p53. The existence of alternative pathways could also explain that, in $Brca1^{S1152A/S1152A}$ MEFs, decreased ATM phosphorylation/activation impacted CHK2 and KAP1 phosphorylation more significantly than that of SMC1 and p53 (Figure 3C). Together, the mutational study of ATM-S1987A strongly suggests that anti-human ATM-pS1981 recognizes mouse ATM that is phosphorylated at a site(s) other than ATM-pS1987. Furthermore, ATM-S1987 is not required for mouse ATM activation.

DISCUSSION

BRCA1 is phosphorylated at multiple serine residues by various DDR-related kinases following DNA damage. Although this observation was among the earliest documented phenomena in BRCA1 research since the cloning of *BRCA1* gene in 1994, the functional role of these phosphorylation sites remained incompletely understood. This is partly due to the fact that posttranslational modifications including phosphorylation often play a role in fine-tuning one particular aspect of multifunctional proteins such as BRCA1. In particular, it is technically challenging to interrogate the impact of these posttranslational modifications on dynamic and reversible processes such as DNA damage response, where DNA repair machinery is assembled and subsequently dissembled after damage is cleared and before normal cell cycle is resumed.

In this study, we continue our investigation on the role of damage-induced BRCA1 phosphorylation in DDR. We show that abrogation of phosphorylation on mouse BRCA1-S1152, which corresponds to ATM phosphorylation site of human BRCA1-S1189, impairs end resection, a commitment step in HR-mediated DSB repair. ATM is believed to be the chief mobilizer in initiating cellular response to DNA double-strand breaks. We demonstrate that, although BRCA1 is phosphorylated by ATM at multiple serine amino acid residues upon DSBs, the S1152A mutation in mouse BRCA1 is sufficient to decrease sustained ATM phosphorylation and activation. This suggests a previously unappreciated feedback loop between BRCA1 and ATM kinase activity, which in turn influences rate of end resection, presumably through its myriad of downstream substrates including MRE11 (Virgilio et al., 2009) (Kijas et al., 2015). We further show that this feedback loop is likely through the SKP2-NBS1-ATM circuit, whereby SKP2-ubiquitinated NBS1 at K63 enhances ATM recruitment and activation and reciprocally, subsequent NBS1 phosphorylation by ATM activates the downstream steps in DDR (Wu et al., 2000). Our results show that BRCA1-S1152A reduces BRCA1 interaction with SKP2 and its recruitment to DBS sites. Recruitment of NBS1 and phospho-ATM is also reduced while assembly of other repair proteins such as MRE11, CtIP, and 53BP1 is not affected.

ATM is a master kinase for orchestrating global cellular responses to DSBs. In human, ATM intermolecular autophosphorylation on S1981 is a critical step in ATM kinase activation (Bakkenist and Kastan, 2003). In addition, ATM autophosphorylation also occurs to other serine residues such as S367 and S1893 (Kozlov et al., 2006) (Kozlov et al., 2015) (Lee and Paull, 2021). Interestingly, autophosphorylation of corresponding mouse ATM on S367, S1899, and S1987 did not seem to be required for mouse ATM activation in transgenic mouse models, in which transgenic expression of ATM-S1987A in *Atm* null mouse restored lymphocyte development and function (Pellegrini et al., 2006) (Daniel et al., 2008). Despite these findings, anti-human ATM-pS1981 antibody has been commonly used in literature as a readout for mouse ATM activation, under the assumption that autophosphorylation at ATM-S1987 is important for mouse ATM activation.

In this study, we show that mouse ATM phosphorylation, as indicated by anti-human ATM-pS1981 antibody, indeed correlates with ATM kinase activity. However, our study of $Atm^{S1987A/S1987A}$ KI MEF cells clearly demonstrates that the phosphorylation detected by this antibody is not related to mouse ATM-pS1987. This antibody therefore likely detects phosphorylation of other ATM serine residues involved in mouse ATM kinase activation, although the exact location of the phosphorylated serine residue(s) in ATM remains to be determined. Consistent with the behavior of previously reported *Atm* null cells

([Pellegrini et al., 2006](#)), the anti-human ATM-pS1981 antibody did not detect any signals in our ATM KO MEF cells. In addition, we show that ATM phosphorylation in response to γ-IR was normal in two independent KI clones of $Atm^{S1987A/S1987A}$ KI MEF cells, making it unlikely that other unknown mutations in the KI MEF clones caused cross reaction with the anti-human ATM-pS1981 antibody. Thus, our current data support the notion that ATM-S1987 is neither involved in mouse ATM kinase activation nor related to mouse ATM phosphorylation detected by anti-human ATM-pS1981 antibody. This helps clarify some of the confusing statements in current literature regarding mouse ATM-S1987.

The impact of BRCA1 phosphorylation on ATM activation and recruitment seems unique to BRCA1-S1152, as BRCA1-S971A does not have the same effect on NBS1 and ATM. Our study therefore suggests that, although multiple phosphorylation sites on BRCA1 by various damage-activated kinases have ultimately promoted HR-mediated DNA repair, each phosphorylation event plays a distinct role in fine-tuning a particular step in the process. Collectively, these individual regulatory events ensure timing, accuracy, and efficiency of DSB repair. Our results also indicate that BRCA1 phosphorylation can influence other DNA repair-related proteins in a feedback loop, adding another layer of intricacy within DNA repair machinery. It is conceivable that communications mediated by phosphorylation and ubiquitination of different DNA repair proteins within the machinery ensures DNA repair to be conducted in an orderly and timely fashion.

Limitations of the study

Although the current study demonstrated that mouse ATM-S1987, which corresponds to human ATM-S1981, is not required for ATM phosphorylation and activity, we are not able to identify which serine amino acid in mouse ATM is detected by the antibody against human ATM-S1981P and is responsible for mouse ATM activity. More systematic research is needed in future to address this issue.

STAR★METHODS

Detailed methods are provided in the online version of this paper and include the following:

- KEY RESOURCES TABLE
- RESOURCE AVAILABILITY
  - ○ Lead contact
  - ○ Materials availability
  - ○ Data and code availability
- EXPERIMENTAL MODEL AND SUBJECT DETAILS
  - ○ Animal housing and ethics
- METHOD DETAILS
  - ○ Generation of immortalized MEF cells
  - ○ Laser micro-irradiation
  - ○ Immunofluorescence (IF
  - ○ Imaging
  - ○ Cell cycle distribution by flow cytometry
  - ○ Co-immunoprecipitation (Co-IP) in HEK293T cells
  - ○ Immunoprecipitation in MEF cells
  - ○ Immunoblotting
  - ○ Generation of ATM-S1987A knock-in (KI) and knock-out (KO) MEFs using CRISPR/Cas9 genome editing system in wild type MEF
  - ○ Generation of $Brca1^{S1152A/S1152A}$ MEF stably expressing full-length wild type human BRCA1 or mouse BRCA1
- QUANTIFICATION AND STATISTICAL ANALYSIS

SUPPLEMENTAL INFORMATION

Supplemental information can be found online at https://doi.org/10.1016/j.isci.2022.104944.

AUTHOR CONTRIBUTIONS

L.Q. and R.C. were responsible for designing and conducting most of the research described in this manuscript. M.L. was responsible for designing and constructing human BRCA1 constructs. C.D. generated BRCA1 KI mouse and was involved in initial discussion of the project. R.L. and Y.H. were responsible for overall design of the project, supervising the project, data analysis, and drafting manuscript.

DECLARATION OF INTERESTS

REFERENCES

Abdulkarim, B.S., Cuartero, J., Hanson, J., Deschênes, J., Lesniak, D., and Sabri, S. (2011). Increased risk of locoregional recurrence for women with T1-2N0 triple-negative breast cancer treated with modified radical mastectomy without adjuvant radiation therapy compared with breast-conserving therapy. J. Clin. Oncol. 29, 2852–2858. http://jco.ascopubs.org/cgi/doi/10.1200/JCO.2010.33.4714.

Bakkenist, C.J., and Kastan, M.B. (2003). DNA damage activates ATM through intermolecular autophosphorylation and dimer dissociation. Nature 421, 499–506.

Blackford, A.N., and Jackson, S.P. (2017). ATM, ATR, and DNA-PK: the trinity at the heart of the DNA damage response. Mol. Cell 66, 801–817.

Cortez, D., Wang, Y., Qin, J., and Elledge, S.J. (1999). Requirement of ATM-dependent phosphorylation of brca1 in the DNA damage response to double-strand breaks. Science 286, 1162–1166.

Daniel, J.A., Pellegrini, M., Lee, J.-H., Paull, T.T., Feigenbaum, L., and Nussenzweig, A. (2008). Multiple autophosphorylation sites are dispensable for murine ATM activation in vivo. J. Cell Biol. 183, 777–783.

Huen, M.S.Y., Sy, S.M.H., and Chen, J. (2010). BRCA1 and its toolbox for the maintenance of genome integrity. Nat. Rev. Mol. Cell Biol. 11, 138–148. https://doi.org/10.1038/nrm2831.

Kijas, A.W., Lim, Y.C., Bolderson, E., Cerosaletti, K., Gatei, M., Jakob, B., Tobias, F., Taucher-Scholz, G., Gueven, N., Oakley, G., et al. (2015). ATM-dependent phosphorylation of MRE11 controls extent of resection during homology directed repair by signalling through Exonuclease 1. Nucleic Acids Res. 43, 8352–8367.

Kim, S.S., Cao, L., Baek, H.J., Lim, S.-C., Li, C., Wang, R.-H., Xu, X., Cho, K.H., and Deng, C.-X. (2009). Impaired skin and mammary gland development and increased r-irradiation-induced tumorigenesis in mice carrying a mutation of S1152-ATM phosphorylation site in Brca1. Cancer Res. 69, 9291–9300.

Kim, S.S., Cao, L., Li, C., Xu, X., Huber, L.J., Chodosh, L.A., and Deng, C.-X. (2004). Uterus hyperplasia and increased carcinogen-induced tumorigenesis in mice carrying a targeted mutation of the Chk2 phosphorylation site in Brca1. Mol. Cell Biol. 24, 9498–9507.

Kozlov, S.V., Graham, M.E., Jakob, B., Tobias, F., Kijas, A.W., Tanuji, M., Chen, P., Robinson, P.J., Taucher-Scholz, G., Suzuki, K., et al. (2015). Autophosphorylation and ATM activation. J. Biol. Chem. 286, 9107–9119.

Kozlov, S.V., Graham, M.E., Peng, C., Chen, P., Robinson, P.J., and Lavin, M.F. (2006). Involvement of novel autophosphorylation sites in ATM activation. EMBO J. 25, 3504–3514.

Lee, J.-H., and Paull, T.T. (2021). Cellular functions of the protein kinase ATM and their relevance to human disease. Nat. Rev. Mol. Cell Biol. 22, 796–814.

Lee, J.-S., Collins, K.M., Brown, A.L., Lee, C.-H., and Chung, J.H. (2000). hCds1-mediated phosphorylation of BRCA1 regulates the DNA damage response. Nature 404, 201–204.

Lim, H.C., Xie, L., Zhang, W., Li, R., Chen, Z.-C., Wu, G.-Z., Cui, S.-S., Tan, E.K., and Zeng, L. (2013). Ribosomal S6 kinase 2 (RSK2) maintains genomic stability by activating the atm/p53-dependent DNA damage pathway. PLoS One 8, e74334.

Lu, Y., Li, J., Cheng, D., Parameswaran, B., Zhang, S., Jiang, Z., Yew, P.R., Peng, J., Ye, Q., and Hu, Y. (2012). The F-box protein FBXO44 mediates BRCA1 ubiquitination and degradation. J. Biol. Chem. 287, 41014–41022. https://doi.org/10.1074/jbc.M112.407106.

Lukas, C., Falck, J., Bartkova, J., Bartek, J., and Lukas, J. (2003). Distinct spatiotemporal dynamics of mammalian checkpoint regulators induced by DNA damage. Nat. Cell Biol. 5, 255–260.

Parameswaran, B., Chiang, H.C., Lu, Y., Coates, J., Deng, C.X., Baer, R., Lin, H.K., Li, R., Paull, T.T., and Hu, Y. (2015). Damage-induced BRCA1 phosphorylation by Chk2 contributes to the timing of end resection. Cell Cycle 14, 437–448.

Pellegrini, M., Celeste, A., Difilippantonio, S., Guo, R., Wang, W., Feigenbaum, L., and Nussenzweig, A. (2006). Autophosphorylation at serine 1987 is dispensable for murine Atm activation in vivo. Nature 443, 222–225.

Polo, S.E., and Jackson, S.P. (2011). Dynamics of DNA damage response proteins at DNA breaks: a focus on protein modifications. Genes Dev. 25, 409–433.

Scully, R., Chen, J., Ochs, R.L., Keegan, K., Hoekstra, M., Feunteun, J., and Livingston, D.M. (1997a). Dynamic changes of BRCA1 subnuclear location and phosphorylation state are initiated by DNA damage. Cell 90, 425–435.

Scully, R., Chen, J., Plug, A., Xiao, Y., Weaver, D., Feunteun, J., Ashley, T., and Livingston, D.M. (1997b). Association of BRCA1 with Rad51 in mitotic and meiotic cells. Cell 88, 265–275.

Shiloh, Y., and Ziv, Y. (2013). The ATM protein kinase: regulating the cellular response to genotoxic stress, and more. Nat. Rev. Mol. Cell Biol. 14, 197–210.

Stracker, T.H., Morales, M., Couto, S.S., Hussein, H., and Petrini, J.H.J. (2007). The carboxy terminus of NBS1 is required for induction of apoptosis by the MRE11 complex. Nature 447, 218–221.

Tian, B., Yang, Q., and Mao, Z. (2009). Phosphorylation of ATM by Cdk5 mediates DNA damage signaling and regulates neuronal death. Nat. Cell Biol. 11, 211–218.

Todaro, G.J., and Green, H. (1963). Quantitative studies of the growth of mouse embryo cells in culture and their development into established lines. J. Cell Biol. 17, 299–313.

Virgilio, M., Ying, C.Y., and Gautier, J. (2009). PIKK-dependent phosphorylation of Mre11 induces MRN complex inactivation by disassembly from chromatin. DNA Repair 8, 1311–1320.

Wu, J., Zhang, X., Zhang, L., Wu, C.-Y., Rezaeian, A.H., Chan, C.-H., Li, J.-M., Wang, J., Gao, Y., Han, F., et al. (2012). Skp2 E3 ligase integrates ATM activation and homologous recombination repair by ubiquitinating NBS1. Mol. Cell 46, 351–361.

Wu, X., Ranganathan, V., Weisman, D.S., Heine, W.F., Ciccone, D.N., O'Neill, T.B., Crick, K.E., Pierce, K.A., Lane, W.S., Rathbun, G., et al. (2000). ATM phosphorylation of Nijmegan breakage syndrome protein is required in a DNA damage response. Nature 405, 477–482.

Yang, J., Qi, L., Chiang, H.-C., Yuan, B., Li, R., and Hu, Y. (2021). BRCA1 antibodies matter. Int. J. Biol. Sci. 17, 3239–3254.

Zhang, J., and Powell, S.N. (2005). The role of the BRCA1 tumor suppressor in DNA double-strand break repair. Mol. Cancer Res. 3, 531–539. https://doi.org/10.1158/1541-7786.MCR-05-0192.

Zhang, J., Willers, H., Feng, Z., Ghosh, J.C., Kim, S., Weaver, D.T., Chung, J.H., Powell, S.N., and Xia, F. (2004). Chk2-phosphorylation of BRCA1 regulates DNA double-strand break repair. Mol. Cell Biol. 24, 708–718.

STAR★METHODS

KEY RESOURCES TABLE

REAGENT or RESOURCE	SOURCE	IDENTIFIER
Antibodies		
Chk1	Santa Cruz	sc-56291; RRID:AB_1121554
p-Chk1 (Ser345)	Cell Signaling	2348; RRID:AB_331212
RPA32	Santa Cruz	sc-28709; RRID:AB_2238546
p-RAP32/34 S4/S8	Bethyl Laboratories	A300-245A; RRID:AB_210547
CHK2	Cell Signaling	2662; RRID:AB_2080793
ATM	Thermo	MA5-14871; RRID:AB_10981520
p-ATM S1981	Rockland antibodies	200-301-400; RRID:AB_217868
H2A.X	Abcam	ab11175; RRID:AB_297814
γH2A.X (Ser139)	Millipore	05-636; :AB_309864
BRCA1	Calbiochem	OP-092;
CtIP	Cell signaling	9201; RRID:AB_10828593
p95/NBS1	Cell signaling	14956; RRID:AB_2798660
K63-linkage Specific Polyubiquitin	Cell signaling	5621; RRID:AB_10827985
SKP2	Cell signaling	2652; RRID:AB_11178941
RAD51	Santa Cruz	sc-8349; AB_2253533
γH2A.X	Cell signaling	9718; RRID:AB_2118009
BrdU	GE Life Sciences	RPN202; RRID:AB_2314032
BRCA1(287.17)	Santa Cruz	sc-135732; RRID:AB_2243740
CtIP	Millipore	RRID: MABE1060;
MRE11	Novus Biologicals	NB100-142; RRID:AB_10077796
SKP2	LSBio	LS-B2487; RRID:AB_2301745
53BP1	MAB3804	Millipore; RRID:AB_2256673
Alexa-488	Life Technologies	A11001; RRID:AB_2534069
Alexa -546	Life Technologies	A10036; RRID:AB_2757557
Alexa-568	Life Technologies	A11036; RRID:AB_10563566
p-H3 (Ser10)	Cell Signaling	9701s; RRID:AB_331535
Chemicals, peptides, and recombinant proteins		
BrdU (5-Bromo-2′-deoxyuridine)	Millipore	19-160
DAPI	Vector Laboratories	H18002
RNase A	Roche	10109169001
Propidium Iodide	Sigma	P4864
NaCl	Fisher	BP358-2121
EDTA	Millipore	324504
NaF	Fisher	S299-100
Na_3VO_4	Fisher	S454-50
Protease inhibitor cocktail	Cell Signaling	58725
Flag M2 magnetic beads	Sigma	M8823
RIPA buffer	Thermo	8990
Protein A/G plus agarose beads	Santa cruz	2003
cOmplete	Roche	30819700
$Na_4P_2O_7.10H_2O$	Fisher	S390

(Continued on next page)

Continued

REAGENT or RESOURCE	SOURCE	IDENTIFIER
DTT	Sigma	D0632
SDS	Invitrogen	AM9820
Cas9	Trilink Bio Technologies	L-7606-100
Triton-X-100	Fisher	BP151
Experimental models: Cell lines		
BRCA1$^{+/+}$ MEF cells	This manuscript	N/A
BRCA1 $^{S1152A/S1152A}$ MEF cells	This manuscript	N/A
HEK293T	N/A	N/A
Experimental models: Organisms/strains		
BRCA1$^{+/S1152A}$ frozen mouse	NIH	N/A
Oligonucleotides		
sgRNA_#1 : AACAGTCCAACATTTGAAGA	This manuscript	N/A
sgRNA_#2 : ACATTTGAAGAAGGAGCTCA	This manuscript	N/A
sgRNA_#3 : TGAGCTCCTTCTTCAAATGT	This manuscript	N/A
sgRNA_#4 : GAAAAAAGTAAAGAAGAAAC	This manuscript	N/A
ATM_sq_6_F : CTGAGTTCTCGTCGCATTATTAC	This manuscript	N/A
ATM_S1987wt.R : CAAACTAGAAATAGTTGTTCCTTGACT	This manuscript	N/A
ATM_S1987A.R : CAAACTAGAAATAGTTGTTCCTTGAGC	This manuscript	N/A
ATM_sq_6_R: GACCTCTGGAAGAGCAGCTAG	This manuscript	N/A
ssODN sequence is: TAACATTGGATAGTATGTT CTCATTAAAAGAGATGTTTTTATGA TAAGCAGAAGTCCAACATTTGAAGA AGGAGCTCAAGGAACAACTATTTC TAGTTTGAGTGAAAAAAGTAAAGAAGA AACTGGAATAAGCTTACAGGTAAATATTAG.	This manuscript	N/A
Recombinant DNA		
pCDH1-mBRCA1	This manuscript	N/A
pCDH1-hBRCA1	This manuscript	N/A
pcDNA3-Flag	This manuscript	N/A
pcDNA3-Flag-BRCA1 (wt)	This manuscript	N/A
pcDNA3-Flag-BRCA1-S1189A	This manuscript	N/A
pcDNA3-Flag-BRCA1-S988A.	This manuscript	N/A
Software and algorithms		
Prism	GraphPad	https://www.graphpad.com/
Fiji	Fiji	https://imagej.net/Fiji
Flowjo	Flowjo	https://www.flowjo.com/
Image Lab	Biorad	https://www.bio-rad.com
Biorender	Biorender	https://biorender.com/

RESOURCE AVAILABILITY

Lead contact

Any request for resources or reagents should be directed to Yanfen Hu (huy3@gwu.edu).

Materials availability

All unique reagents generated in this study are available from the lead contact with a completed materials transfer agreement.

Data and code availability

All data reported in this paper will be shared by the lead contact upon request. This paper does not report original code. Any additional information required to reanalyze the data reported in this paper is available from the lead contact upon request.

EXPERIMENTAL MODEL AND SUBJECT DETAILS

Animal housing and ethics

All animal related experiments were approved by Institutional Animal Care and Use Committee (IACUC) at University of Texas Health San Antonio (2007–2018) and The George Washington University (2018-present).

METHOD DETAILS

Generation of immortalized MEF cells

BRCA1$^{+/S1152A}$ frozen mouse embryos at 8-cell stage were obtained from NIH under specific MTA and frozen embryos were revived to give live mice and their genotype was confirmed. Mouse embryos (13.5–14.5 days postcoitum) generated from intercrosses between *BRCA1*$^{+/S1152A}$ mice were dissected and internal organs removed as described earlier (Yang et al., 2021). Genotyping of MEF cells was initially performed using residual embryo tissues and confirmed multiple times in the process of immortalization. WT and *Brca1*$^{S1152A/S1152A}$ MEF cells derived from littermate embryos were immortalized using the regular 3T3 protocol (Todaro and Green, 1963).

Laser micro-irradiation

In a standard laser microirradiation protocol, BrdU is incorporated in chromatin DNA before cells are subject to microirradiation (Lukas et al., 2003) (Polo and Jackson, 2011). We made a minor modification of the protocol. i.e. we incubated MEF cells in the presence of BrdU only for two hours before microirradiation, rather than incubation with BrdU for overnight or 24-hours as commonly used in the field. The laser output was set at an energy level that DSBs could be generated only when DNA incorporated BrdU. In other words, microirradiation generated DSBs in a BrdU-dependent manner under this condition. This was confirmed and described in our previous work (Parameswaran et al., 2015), as demonstrated by the detection of gH2AX stripes, a readout for presence of DSBs, only when cells were preincubated with BrdU. Generation of DSBs by microirradiation in a BrdU-dependent manner, in combination with a transient 2-hours BrdU preincubation, ensures DSBs were generated only in the S/G2 cells even though the cells seeded were asynchronous. This design allowed us to conveniently examine accurate end resection kinetics in S/G2 cells, when end resection normally occurs, and effectively avoid generating DSBs in G1 cells, when end resection does not happen in principle.

DSBs can also be generated by laser microirradiation in a BrdU-independent manner, when higher laser output is used (Parameswaran et al., 2015). It is conceivable that BrdU-incorporated DNA might form less compacted DNA and therefore requires lower energy level to generate breaks. In contrast, normal DNA is densely compacted and needs higher laser energy to produce DSBs compared to BrdU-incorporated DNA. When DSBs are generated by BrdU-independent microirradiation, it is not necessary to preincubate cells in the presence of BrdU. Under this condition, every cell subject to microirradiation would produce DSB stripes, regardless whether DNA incorporated BrdU or not. In our BrdU-independent microirradiation, MEF cells were still preincubated with BrdU for 24 hours (same as in a standard microirradiation protocol) so that BrdU was incorporated into DNA in every cell. The purpose of BrdU incorporation in this context is to serve as a readout for end resection. The detection of BrdU by its antibodies in undenatured DNA reflects ongoing and/or completed end resection in these cells at DSBs.

MEF cells were plated on 8-well Nunc Lab Tek II chamber slides and pre-treated with or without 50 µM BrdU for durations as indicated. Wells with ~70–80% cell confluency were chosen for micro-irradiation. Micro-irradiation was performed using a MMI Cell Cut laser micro-dissection system consisting of a 390 nm ND-YAG laser that is coupled to the optical path of a microscope. The details have been previously described (Parameswaran et al., 2015).

Immunofluorescence (IF

Chamber slides were fixed at indicated times after micro-irradiation with either 3% paraformaldehyde/2% sucrose in phosphate buffer saline (PBS), pH 7.4 at room temperature (RT) for 15 min or 70% Methanol/30%

Acetone at −20°C for 15 min. Cells were washed and treated as previously described (Parameswaran et al., 2015). Primary antibodies were detected using specific secondary antibodies conjugated with Alexa-488 (1:1000 or 1:200), Alexa-546 (1:500) or Alexa-568 (1:200) (Molecular Probes, Life Technologies) at RT for 2 hours. Cells were then washed twice with 1XPBS at RT for 5 min and were mounted with a 24 × 50, #1.5 coverslip using Vectashield with DAPI (Vector Laboratories). All immunostained slides were visualized using Zeiss LSM710 confocal microscope.

Imaging

ImageJ software was used for the purpose of laser stripe intensity quantification. Straight line tool (line width = 20) was used to draw lines over all γH2AX stripes and the intensities of corresponding BRCA1 stripes were measured.

Cell cycle distribution by flow cytometry

For BrdU/PI labeling, $Brca1^{WT}$ and $Brca1^{S1152A/S1152A}$ MEF cells were pulse-labeled with 50 μM BrdU for 1 hour. After trypsinization, cells were washed in 1XPBS containing 1%FBS and 1% Sodium azide (PBS/S/N), then fixed in pre-chilled 90% ethanol, followed by washing in PBS/S/N solution to remove ethanol. Cells were then treated with 2M HCl and incubated at RT for 20 min, washed in wash buffer (PBS/0.5% Tween-20/0.5% BSA) followed by neutralization with 0.1M Boric Acid, pH 8.5 at RT for 5 min. Cells were washed and then stained with Alexa Fluor- 488 conjugated anti-BrdU (1:100, GE Healthcare) at 37°C for 30 min in the dark. Cells were then washed and incubated in PBS containing 25μg/mL Propidium Iodide (Sigma) and 25μg/mL RNase A (Roche) at RT for 30 min followed by flow cytometric analysis.

For detection of phosphorylated histone H3ser10, ethanol-fixed cells were permeabilized with 0.25% Triton-X-100 in PBS on ice for 15 min, washed and stained with anti-phospho-Ser10 histone H3 antibody (1:50, Cell Signaling Technology) for 1 hour at 37°C. This was followed by incubation of Alexa Fluor 488-conjugated anti-rabbit secondary antibody (1:500, Molecular Probes) at 37°C for 1 hour in the dark. Cells were washed and incubated with PI for 30 min prior to flow cytometry analysis. All data were collected using FACS Calibur (Becton Dickson) and analyzed using Flowjo software.

Co-immunoprecipitation (Co-IP) in HEK293T cells

HEK293T cells (2×10^6 cells/6-cm dish) were transfected with pcDNA3-Flag (vector control), pcDNA3-Flag-BRCA1 (wt), pcDNA3-Flag-BRCA1-S1189A or pcDNA3-Flag-BRCA1-S988A. 24 h post-transfection, cells from one 6-cm dish were split into two 10-cm dishes. 24 h post re-seeding, one of the two plates was subjected to 20Gy IR. Cells were incubated at 37°C for 30 min before harvesting. Cells were lysed by rotating at 4°C for 30 min in 500 μL of NETN lysis buffer (150 mM NaCl, 1 mM EDTA, 20 mM Tris HCl, pH 8.0, 0.5% NP-40, 5 mM NaF, 2 mM $Na_4P_2O_7.10H_2O$, 2 mM Na_3VO_4, 1 mM PMSF, cOmplete, Mini, EDTA-free Protease inhibitor cocktail from Roche)). Lysed cells were passed through 21G needle 10–12 times, and then clarified by centrifugation at 14,000 rpm for 10 min at 4°C. Protein quantification using BCA kit (following the company protocol) was performed and approximately 600 μg of lysate was used for IP with anti-Flag M2 magnetic beads (#M8823, Sigma). The samples were then resolved by SDS-PAGE followed by immunoblotting.

Immunoprecipitation in MEF cells

$Brca1^{WT}$ and $Brca1^{S1152A/S1152A}$ MEF cells (6×10^6 cells each) and $Brca1^{WT}$ and $Brca1^{S971A/S971A}$ MEF cells (6×10^6 cells each) were subjected to no IR or 10 Gy IR and incubated at 37°C for 1 hour before harvesting. Cell pellets were lysed in 500–1000 μL RIPA buffer and lysates were passed through 21G needle 10–12 times and were clarified by centrifugation at 14,000 rpm for 10 min. Protein quantification using Pierce BCA kit was performed per the manufacturer's protocol and approximately 1000–1500 μg of sample was pre-cleared with 20 μL Protein A/G plus agarose beads (#2003, Santa cruz) at 4°C for 30 min and IP'ed with anti-p95/NBS1 (D6J51)or irrelevant anti-rabbit antibody as a control. On following day, 20 μL of Protein A/G plus agarose beads were added and allowed to combine at 4°C for 4 h. Samples were resolved by SDS-PAGE followed by immunoblotting.

Immunoblotting

Following experimental conditions, cells were lysed in 2X Laemmli buffer (100 mM Tris pH6.8, 200 mM DTT, 4% SDS, 20% glycerol, 0.2% BPB) and boiled for 10 min. Samples were resolved in 5–15% SDS-PAGE and

electrophoretically transferred into nitrocellulose or polyvinylidene difluoride (PVDF) (for ATM blots) membranes. Membranes were blocked in 5% milk-TBST and probed with primary antibodies described in the table below.

Generation of ATM-S1987A knock-in (KI) and knock-out (KO) MEFs using CRISPR/Cas9 genome editing system in wild type MEF

Four sgRNA oligos for generating DSBs in *Atm* gene locus around ATM-S1987 position were designed and selected from the Benching or Broad Institute platform. Two million wild type MEF cells were transfected with sgRNA (12 μg), Cas9 (20 μg, Trilink Bio Technologies, L-7606), ssODN (single-stranded oligodeoxynucleotides as the template in HR mediated repair process, 26 μg, IDT) mixture using Nucleofector 2b following the Nucleofector kit (Lonza, VPD-1005) protocol. Cells were re-seeded in 96-well plates (0.8 cell/well) one day after transfection and single-cell clones were screened for desired KI and KO at *ATM* locus. All KI or KO clones were screened by PCR first (using primers ATM_sq_6_F with either ATM_S1987 wt.R or ATM_S1987A.R) and then confirmed by sequencing (GENEWIZ, PCR primer used for this step is ATM_sq_6_F and ATM_sq_6_R.

Generation of *Brca1*$^{S1152A/S1152A}$ MEF stably expressing full-length wild type human BRCA1 or mouse BRCA1

Brca1$^{S1152A/S1152A}$ MEF cells were transfected with either pCDH1-hBRCA1 or pCDH1-mBRCA1 following the Nucleofector kit protocol (Lonza, VPD-1005) and selected by Puromycin (Gibco, A1113803) 2 days after transfection. Overexpression of exogenous full-length BRCA1 in pooled cells was examined and confirmed by BRCA1 Western blotting.

QUANTIFICATION AND STATISTICAL ANALYSIS

Each graph is quantification of several independent experiments, acquired either on different days or performed by different scientists as indicated in the figure legends. All statistical analyses were performed using Microsoft Excel. Unpaired students t-test was performed to generate p values indicative of statistical significance. p-value: No significance (ns); $p<0.05$ (*); $p<0.01$ (**); $p<0.001$ (***).